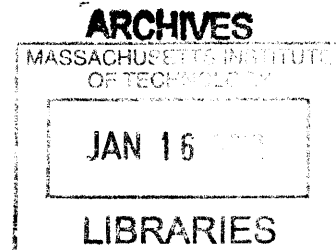# An Injection-Locked 674 nm Laser for Strontium-88 Ion Trapping

by

Rena J. Katz

Submitted to the Department of Physics
in partial fulfillment of the requirements for the degree of

Bachelor of Science in Physics

at the

MASSACHUSETTS INSTITUTE OF TECHNOLOGY

June 2012

© Rena J. Katz, MMXII. All rights reserved.

Author . . . .
Department of Physics
May 15, 2012

Certified by . . . .
Isaac L. Chuang
Professor of Physics
Professor of Electrical Engineering and Computer Science
Thesis Supervisor

Accepted by . . . .
Nergis Mavalvala
Professor of Physics
Thesis Coordinator

An Injection-Locked 674 nm Laser for Strontium-88 Ion Trapping

by

Rena J. Katz

Submitted to the Department of Physics
on May 15, 2012, in partial fulfillment of the
requirements for the degree of
Bachelor of Science in Physics

Abstract

Energy levels of the valence electron of a single trapped $^{88}\mathrm{Sr}^{+}$ ion can be harnessed as an effective qubit for quantum information processing. The qubit transition to a metastable energy state can be stimulated by a laser at a frequency of 444.779044 THz. A laser beam with higher intensity causes more rapid transitions between quantum states, and thus allows more computational operations within the coherence time of the system. The focus of this thesis is the design and construction of a more powerful laser to stimulate the qubit transition of the $^{88}\mathrm{Sr}^{+}$ ion, using injection-locking to stabilize the frequency of the new laser.

Injection-locking is a technique for using an existing, stable laser to control the frequency of a second laser diode. A small amount of input power is enough to produce a much more powerful output beam at the same frequency, so the system acts as an amplifier. We found that a AlGaInP laser diode required 9 ± 2 μW of injected input power to lock to the input frequency, producing an output power of 11.56 ± 0.31 mW. The ratio of input to output power was $(7.8 \pm 1.7) \times 10^{-4}$. The injection-locking frequency range was 18.4 ± 1.6 MHz.

Thesis Supervisor: Isaac L. Chuang
Title: Professor of Physics
Professor of Electrical Engineering and Computer Science

Acknowledgments

I've learned so much from the time I have spent working in the Quanta Lab, particularly from working with everyone. I want to thank everyone in the lab for making this research experience fascinating and worthwhile for me.

Ike has been a great advisor, giving timely advice and suggestions both on the details of my project and guiding the overall direction. I have learned so much about physics from brief conversations (not to mention Junior Lab orals) with Ike. I appreciate that he has held my work to such a high standard that I have learned more than I thought possible.

Peter, with his detailed knowledge of every component of a laser, offered crucial pieces of advice that allowed me to demonstrate injection-locking. He is always encouraging and willing to take the time to help out, but also made sure that I accomplished the physical work entirely on my own.

Amira's knowledge of electronics and the existing laser systems was extremely helpful when I started work on the automatic frequency controller. She is always available to answer questions about the experimental setup in lab or to point me towards useful references for electronics. Her dedication is inspiring.

Shannon and Arolyn both offered excellent advice and proofreading on several occasions. Shannon has helped me understand some difficult quantum computing concepts. Arolyn has given me some great life advice for grad school and the application process.

Joan was the best Junior Lab partner I could have asked for, and continues to be a great friend. She got me started with Python data analysis and computerized data collection, which I continued to learn about and use in the Quanta Lab.

Sean, my boyfriend, has been a great source of encouragement and is always willing to help me talk through the best course of action for approaching many problems.

My parents have always been supportive of me and my work. Their confidence in me and their willingness to both listen and give advice when I am going through a rough time has sustained me through my time at MIT.

Contents

List of Figures

Chapter 1

Introduction

1.1 Physical systems for quantum information processing

A classical computer stores and manipulates information that can be represented by binary numbers. A single bit in a classical computer can be in either an "on" or "off" state. Logic gates which act on the bit can change its value between the "on" and "off" states. Quantum computers are not limited to storing information in two discrete, well known states. A quantum computer can store and manipulate information using a system which can be in a range of superposition or entangled quantum states. When measured, the system will be found in one of two states, analogous to the "on" and "off" states of the classical bit. The two orthogonal quantum states are usually represented by $|0\rangle$ and $|1\rangle$. The system can be in a superposition of these two states, and the states of two or more systems may be entangled. Such a quantum system is called a "qubit."

Many different physical systems can be harnessed as qubits. Quantum algorithms have been demonstrated on systems ranging from the macroscopic, such as the ensemble of nuclear spins in a liquid sample probed by NMR [CVZ+98, VSB01], to the microscopic, such as the electron energy levels of trapped ions [MMKI95, GRL+03]. The challenge facing large-scale quantum computing is that systems harnessed as

qubits tend to be highly sensitive to their environment and require bulky, expensive equipment to maintain just a few qubits. The dream for quantum information processing technology is the invention of the analogue of the transistor: a cheap, reliable, scalable device which can store and manipulate quantum information.

Trapped ions can be used as excellent qubits due to their long coherence time and ease of control with lasers. An ion trapping system can be scaled up to include many trapped ions [KMW02]. Individual ions in a linear ion trap can be controlled independently with laser addressing [NLR+99]. Although trapped ions can be used as effective qubits on their own, they can also be readily combined with other quantum systems. For example, trapped ions can be entangled with photons so that information can be transmitted over long distances [BMD04], and it has been theoretically proposed that a trapped ion could be coupled to a superconducting qubit to increase the speed of calculations [TRBZ04].

A single ion can be held in place by electrodes producing radio frequency (RF) and DC electric fields which combine to create a pseudopotential well. Static electric fields cannot produce a potential with a stable minimum in free space [Pau90]. This would require an attractive charge in the desired location to hold the ion. The best that a DC electric field can produce is a saddle-shaped quadrupole potential, with stable oscillatory behavior of the ion along the axis between two repulsive electrodes and unstable escape behavior along the perpendicular axis between two attractive electrodes. An oscillating RF saddle-shaped potential is used instead. An ion with sufficiently low kinetic energy will not escape the time-dependent electric field because the axis of stability is constantly changing.

An ion must be cold enough (have small enough kinetic energy) to not escape the pseudopotential well of the ion trap. Ion trapping is often performed in ultra-high vacuum to minimize the influence of environmental interactions on the ion. Typically, ions are trapped at room temperature; however, if they are trapped at cold temperatures (~ 6 K), the heating rate of the ion is greatly reduced, as shown in a measurement by Labaziewicz et al. [LGA+08]. Reducing the heating rate of the ion is important for trapping ions within a more compact space, because a smaller distance

between the ion and the trap causes heating rates to increase. To maintain the ion in the trap, it is laser cooled. To maintain an ion in a trap in a particular quantum state, lasers of specific wavelengths are required both for laser cooling and for manipulating the state of the qubit. The lasers must be tuned to sufficiently precise frequencies and be intense enough to stimulate and saturate transitions in the ion.

1.2   Using the ^{88}Sr$^+$ ion as a qubit

For a trapped ion to function as an effective qubit, it must be able to maintain a $|0\rangle$ or $|1\rangle$ state with a long coherence time. The experimentalist must be able to modify and read out the value of the state in order to store information and perform calculations. The ^{88}Sr$^+$ ion is a good candidate for creating a qubit because it has a metastable state with a long coherence time (≈ 390 ms) and the relevant states are easily accessible using visible and infrared diode lasers. Fig. 1-1 shows the relevant energy levels used to access the qubit transition. The S-P and P-D transitions are electric dipole transitions, with fast decay rates. The transition between the $4D_{5/2}$ metastable state and the $5S_{1/2}$ ground state is an electric quadrupole transition, with a much lower spontaneous decay rate, stimulated by a 674 nm laser. These two sets of transitions can be accessed independently of each other, so the fast transition involving $5P_{1/2}$ can be used for laser cooling and the metastable state $4D_{5/2}$ can be used for information storage, without these two processes affecting each other.

Increased laser power for stimulating the qubit transition increases the frequency of Rabi oscillations. Rabi oscillations are a periodic cycle between the ground state ($|0\rangle$) and excited state ($|1\rangle$) of the valence electron, due to absorption and stimulated emission of photons. A greater intensity of photons in the beam increases the speed of the process, up to a saturation limit. Increasing the frequency of Rabi oscillations reduces the time needed to induce a transition to the metastable $|1\rangle$ qubit state, allowing quantum calculations to be performed more quickly, thus permitting more quantum operations within the coherence time of the system.

To load strontium into the ion trap, a vapor of neutral atoms is produced, which

are then photoionized by a two photon process requiring two lasers. One or more photoionized atoms can then be captured by the trap. The first step in the process consists of an electron in the $(5s^2)^1S_0$ ground state excited to the $(5s5p)^1P_1^0$ state by a dipole transition, stimulated by a 461 nm laser. The second step is to bring the electron to an autoionizing $(5p^2)^1D_2$ state with a 405 nm laser. This autoionizing state will quickly decay into an ion and a free electron, the desired configuration.
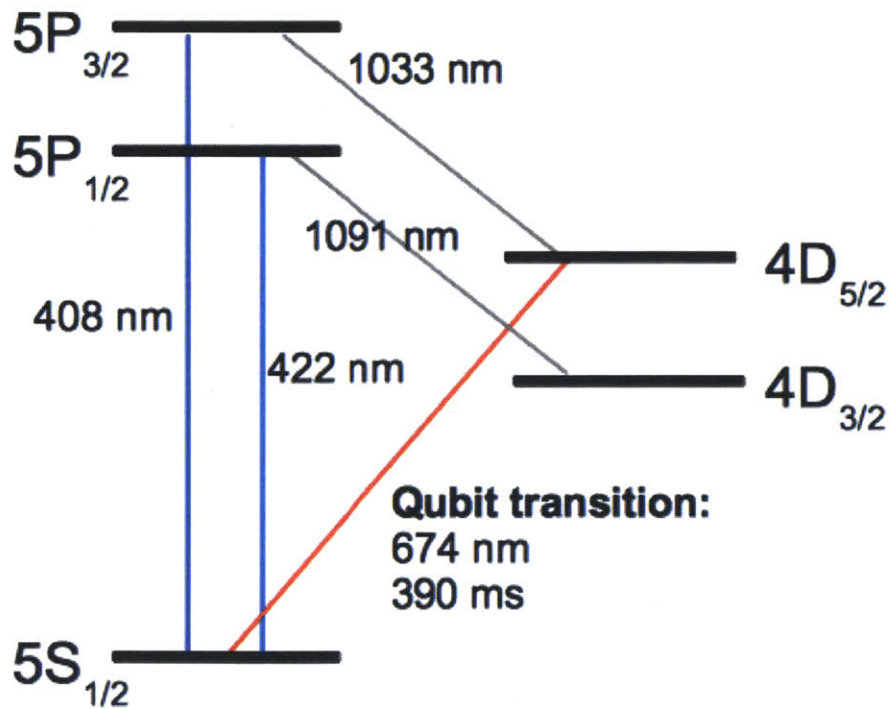
Figure 1-1: Relevant states of the ^{88}Sr$^+$ ion for quantum information processing. The qubit transition, from the 5S$_{1/2}$ state to the 4D$_{5/2}$ state is stable for a much longer time than the other transitions: 390 ms as compared to nanoseconds for the other transitions.

1.3   Laser cooling of the trapped ion

Heating of the trapped ion corresponds to increased random motion, which means that the ion is more likely to escape the trap. If the ion has only one quantum of kinetic energy, it is said to be in the motional ground state. For good stability and coherence times, trapped ions must be held near their motional ground state.

Laser cooling decreases the kinetic energy of an ion through a process in which the ion absorbs and emits photons. When the ion is moving with respect to the laser beam, the photons appear Doppler shifted to the ion. The ion can absorb a photon with the correct Doppler shifted frequency to stimulate a transition between energy levels. When the electron later decays back to the ground state, the frequency of the photon will not be Doppler shifted with respect to the ion and thus the emitted photon may have a lower energy than the absorbed photon. A laser of wavelength 422 nm is used to stimulate the transition between the $5S_{1/2}$ and $5P_{1/2}$ states for laser cooling of the ion.

An order of magnitude calculation can be used to estimate how much energy an ion gains when it heats up in a trap. The ion is trapped in approximately a harmonic oscillator potential, $V(x)$.

$$V(x) = \frac{1}{2}m\omega^2 x^2 = 2m\pi^2\nu^2 x^2 \qquad (1.1)$$

where m is the ion's mass, ω is the angular frequency, and x is the position coordinate. We estimate ν, the frequency, to calculate a change in energy in the harmonic oscillator: $h\nu$, where h is Planck's constant. Setting the corresponding energy qV_0 equal to the harmonic oscillator potential energy and solving for ν gives:

$$\nu = \sqrt{\frac{qV_0}{2\pi^2 m x^2}} \qquad (1.2)$$

The potential depth of the trap V_0 is on the order of 1 V. Plugging in $q/m = 2.2 \times 10^6$ C/kg for a strontium ion and $x \sim 0.1$ mm as an approximate width of the potential gives $\nu \sim 1$ MHz. The temperature change due to heating of the ion can be estimated

from

$$h\nu = k_B T \tag{1.3}$$

where h is Planck's constant and k_B is Boltzmann's constant. $T \sim 10^{-4}$ K, a tiny temperature change.

1.4 My thesis contributions

The work presented in this thesis focuses on improving the performance of the laser used for stimulating the qubit transition of trapped $^{88}\mathrm{Sr}^+$ ions in the Quanta Lab. The power of the 674 nm laser in the Quanta Lab was not sufficient when shared among multiple experiments simultaneously using the $^{88}\mathrm{Sr}^+$ ion as a qubit. Chapter 3 describes the design and construction of an injection-locked laser which amplifies the output of the 674 nm laser.

I collaborated with others in lab and received helpful guidance on the design of the injection-locked laser setup. The majority of the hands-on and programming work is my own, with the exceptions that the general design and some of the equipment selection was completed by others before I joined the project, and I have repurposed sections of code that had already been written to interface with hardware devices such as the wavemeter or power supply.

Chapter 2

Relevant theory for an injection-locked laser

2.1   Introduction

Injection-locking of a laser was first demonstrated by H. L. Stover and W. H. Steier from Bell Labs, in 1966 [SS66]. The technique has become common for building stable lasers with accurate frequencies in physics labs. An injection-locked laser amplifies a beam from an existing, stable laser (the master laser) by directing the beam into another laser diode (the slave laser) to produce an amplified output at the same frequency. Section 2.2 describes how the slave laser can be modeled as an oscillator, and how the effect of injecting a master beam can be modeled as a driven oscillator. One of the major challenges of setting up an injection-locked laser is to align and shape the two beams precisely so that they overlap and have similar dimensions along their beam paths. Section 2.3 discusses ray optics and Gaussian beam propagation, which can be used to model the beam path and determine what lenses are needed to shape the beams.

2.2 Theory of injection-locking

Injection-locking is so called because the technique uses an injected laser beam from the master laser to lock the frequency of the slave laser. Similar to the effect of a grating in an external cavity diode laser, the injected beam constrains the output to a particular frequency, if the injected frequency is close enough to the free-running, unconstrained frequency.

The following discussion is based on Siegman [Sie86]. A free running laser diode can be thought of as an oscillator, with frequency ω_0 and coherent output intensity I_0. When a low power signal at frequency ω_1 is injected into the diode, if ω_1 is outside the locking range, the output from the laser will contain two signals: one from the free-running oscillator at frequency ω_0 and one from the master injected signal at frequency ω_1. The system reaches a resonance in amplitude at $\omega_1 = \omega_0$. To model this resonance, it is useful to develop a model based on an amplifying interferometer cavity with round-trip gain of $G(\omega)$, capped with a mirror that is partially transmitting with reflectance R. The gain of the diode medium as a function of the injected frequency is $|g(\omega_1)|^2$, where $g(\omega_1)$ is

$$g(\omega_1) \approx \frac{1 - R}{1 - G + jGT(\omega_1 - \omega_0)}. \tag{2.1}$$

T is the round-trip transit time of the beam through the cavity, and $j = \sqrt{-1}$. If the master frequency is tuned closer to the free-running frequency, the amplification of the injected master signal will increase as it approaches resonance at $\omega_1 = \omega_0$. However, the total intensity emitted from the diode cannot exceed I_0 plus the intensity of the injected beam. The amplified master signal will overpower the free-running signal since the gain medium can only produce a limited total intensity. Inside the locking range, the output will consist entirely of a signal at the master frequency, ω_1, with an approximate intensity of I_0.

The injection locking range is the range of the master frequency for which the output intensity at the frequency of the master laser is equal to I_0 and the free-running output signal is suppressed. The injected power from the master laser is I_1

and the gain is $|g(\omega_1)|^2$, so the injection locking range is the range of frequencies for which this relation holds:

$$|g(\omega_1)|^2 = \frac{\gamma_e^2}{(\omega_1 - \omega_0)^2} I_1 \approx I_0 \tag{2.2}$$

where γ_e^2 is the external decay rate, a measure of how much power is lost through external coupling of the cavity during each round-trip oscillation. The external decay rate is given by:

$$\gamma_e^2 = \frac{\omega}{Q_e} \tag{2.3}$$

where Q_e is the Q-factor for the external cavity and ω is the frequency of the light oscillating inside the cavity. Substituting this relation for γ_e^2 into the equation for the injection locking range gives

$$\Delta\omega_{lock} \approx \frac{2\omega_0}{Q_e}\sqrt{\frac{I_1}{I_0}}. \tag{2.4}$$

The factor of 2 is due to the injection locking range extending both above and below ω_0. Although this equation was derived from an external cavity diode laser model, this model can be applied to many different kinds of injection-locked oscillators.

The injection-locking range of laser diodes has been theoretically calculated and experimentally measured. Bour and Rosen calculated the optimum cavity length for a quantum well diode laser with output coupling of 10% to be approximately 360 μm [BR89]. Based on an estimate in Siegman [Sie86] we can estimate the injection locking range of such a laser cavity:

$$\frac{\Delta\omega_{lock}}{2\pi} \approx 14\text{GHz} \times \sqrt{\frac{I_1}{I_0}}. \tag{2.5}$$

For $I_1/I_0 = 1/1000$, $\Delta\omega_{lock}/2\pi = 440$ MHz. Clarke, Riis, et al. experimentally measured a locking capture range of about 800 MHz which varied linearly with injected power for a semiconductor laser diode with an output near 674 nm [CRB98]. Because factors such as the quality factor Q of the laser cavity, the length of the cavity, the ratio of injected to output intensity, and the alignment of the injected beam as it enters the slave diode can be expected to vary in the experimental setup, these calculations

21

should be treated as a rough estimate.

The slave diode can be modeled as a driven oscillator, with a natural frequency ω_0 and a driving frequency ω_1. The time-varying amplitude of the electric field inside the cavity $E(t)$ can be described by two fundamental injection-locking equations [Sie86]:

$$\frac{dE(t)}{dt} + \frac{\gamma_c - \gamma_m}{2} E(t) = \gamma_e E_1(t) \cos\left[\phi(t) - \phi_1(t)\right] \tag{2.6}$$

$$\frac{d\phi(t)}{dt} + \omega_1 - \omega_0 = -\gamma_e \frac{E_1(t)}{E(t)} \sin\left[\phi(t) - \phi_1(t)\right] \tag{2.7}$$

where $E(t)$ is the amplitude of the cavity signal, $E_1(t)$ is the amplitude of the injected signal, γ_c and γ_m are the total cavity decay rate and the amplitude growth rate, and $\phi(t)$ and $\phi_1(t)$ are the time dependent phase of the signal inside the cavity and the injected signal, respectively. If the injected signal vanishes ($E_1(t) \to 0$), the equations simplify: the amplitude oscillates at the natural frequency and the phase ϕ remains constant. The injected signal can modify the amplitude, the phase, and the frequency of the output signal.

2.3 Optics

2.3.1 Ray optics and matrices

Modeling beam paths and the effect of lenses is important in order to overlap the master and slave beams along their lengths with matching beam radii. A matrix formulation of a propagating light ray is an effective model for determining the radius and divergence along a beam. The following discussion is based on Siegman [Sie86]. A ray of light can be described by two parameters: $r(z)$ and $r'(z)$, where z is the optical axis and r is the perpendicular displacement from the optical axis. $r'(z)$ is essentially the slope of the ray, but it also takes into account the index of refraction $n(z)$: $r'(z) = n(z)\frac{dr(z)}{dz}$.

As the ray propagates through free space or optics, its position and slope can change. These changes are modeled by matrices as follows, where r_1 and r'_1 are the

original position and slope of the ray and r_2 and r_2' are the position and slope after propagation:

$$\begin{bmatrix} r_2 \\ r_2' \end{bmatrix} = \begin{bmatrix} A & B \\ C & D \end{bmatrix} \begin{bmatrix} r_1 \\ r_1' \end{bmatrix}. \qquad (2.8)$$

The entries in the ABCD matrix must obey the relation $AD - BC = 1$. The values A, B, C, and D are selected to model the desired change to the position and divergence. For an elliptically shaped beam, the x- and y- components of the ray vector may be propagated separately using $x(z)$ and $y(z)$ vectors instead of an $r(z)$ vector. To describe a cylindrical lens with focal length f, we can use the matrix describing a thin lens, acting on one of the components of the ray perpendicular to the optical axis [Gol86].

$$\begin{bmatrix} x_2 \\ x_2' \end{bmatrix} = \begin{bmatrix} 1 & 0 \\ -1/f & 1 \end{bmatrix} \begin{bmatrix} x_1 \\ x_1' \end{bmatrix} \qquad (2.9)$$

The other component $y(z)$ of the ray does not change (or equivalently, it is propagated with the identity matrix).

2.3.2 Gaussian beam propagation

While ray optics are sufficient to describe a beam in its linear regime, far from a focus, the Gaussian beam model can be used to characterize a beam by its behavior near a focus. The following discussion is based on Siegman [Sie86]. Assuming that a Gaussian beam has both a smallest width (beam waist) of w_0 and an infinite radius of curvature $R(z)$ at $z = 0$, the propagation of the beam can be modeled as:

$$\tilde{u}(x, y, z) = \left(\frac{2}{\pi} \right)^{1/2} \frac{\tilde{q}_0}{w_0 \tilde{q}(z)} \exp\left(-jkz - jk\frac{x^2 + y^2}{2\tilde{q}(z)} \right) \qquad (2.10)$$

where $k = \omega/c$, and the complex radius of curvature $\tilde{q}$ is defined by:

$$\frac{1}{\tilde{q}(z)} = \frac{1}{R(z)} - j\frac{\lambda}{\pi w^2(z)} \qquad (2.11)$$

where $j = \sqrt{-1}$, and q_0 is the complex radius of curvature at $z = 0$. The spot size of the beam, $w(z)$, is the radius at which the amplitude of the electric field drops to $1/e$ of the value at the optical axis. It can be expressed as:

$$w(z) = w_0 \sqrt{1 + \left(\frac{z}{z_R}\right)^2}. \tag{2.12}$$

The minimum value of $w(z)$ is $w_0 = w(z = 0)$ and is called the beam waist. The Rayleigh range z_R describes how quickly the beam diverges from the beam waist. It is defined as $z_R = \frac{\pi w_0^2}{\lambda}$. At $z = z_R$, the spot size of the beam is $\sqrt{2}w_0$. The radius of curvature is:

$$R(z) = z + \frac{z_R^2}{z} \tag{2.13}$$

A beam after passing through a thin lens will have a radius of curvature equal to the focal length of the lens. Once the beam waist is known, the spot size and radius of curvature can be calculated for any value of z. If the beam waist is smaller, the beam will diverge more rapidly. The lens law for gaussian beams (directly analogous to the familiar lens equation) is:

$$\frac{1}{\tilde{q}_2} = \frac{1}{\tilde{q}_1} - \frac{1}{f} \tag{2.14}$$

where $\tilde{q}_1$ and $\tilde{q}_2$ are the complex radii of curvature of the beam before and after the lens.

Although the perfect Gaussian beam is a useful model, in reality a laser beam will not be exactly Gaussian. It is useful to quantize how closely a beam's shape matches the Gaussian model. The beam quality parameter M^2 describes how close the beam is to a perfect Gaussian shape. It is defined as

$$\theta = M^2 \frac{\lambda}{\pi w_0} \tag{2.15}$$

where θ is the half-angle beam divergence, λ is the wavelength, and w_0 is the beam waist. In the limit of a perfect Gaussian beam, $M^2 = 1$. An actual beam will have $M^2 > 1$.

Chapter 3

Construction of
an injection-locked laser

3.1 Introduction

This chapter describes the experimental portion of the injection-locked laser project,
including the design, testing, and selection of equipment (Section 3.2) and a demon-
stration of injection-locking (Section 3.3). The overall design of the setup and the
selection of most parts other than the laser diode, diode mount, beam shaping lenses,
and temperature controller were done by other lab members before I joined the
project. My contributions involved testing several laser diodes, implementing effective
temperature control, installing and aligning lenses for beam shaping and mode match-
ing, and determining temperature and current settings such that the free-running
frequency output of the diode was close enough to the injected frequency for injection
locking.

3.2 Design

3.2.1 Overview of the setup

An injection-locked laser in general requires an input from the master laser, a powered and temperature controlled slave diode, an optical isolator to prevent backpropagation of the light into the master laser, and lenses and mirrors sufficient to collimate, shape, and align the master and slave beams. A schematic of the setup is shown in Fig. 3-1 and a photograph of the setup is shown in Fig. 3-2. The injected master beam and the slave beam from the diode must overlap and have the same shape. The beam exiting the diode is first focused by a spherical collimating lens. However, since the diode emits an elliptical beam, a telescope constructed from cylindrical lenses is required to produce a round beam. The injected beam from the master laser was already approximately collimated, but it had a larger diameter than the slave beam. A telescope of spherical lenses is used to match the diameters of the two beams. The frequency of the master and slave beams are measured by a High Finesse WS-7 wavemeter.

3.2.2 Laser diode

Due to slight variations in the manufacturing process, the output frequency as a function of temperature and current of each individual laser diode (even among diodes from the same batch) will vary slightly. We tested several diodes before finding one that could output the desired frequency. The testing process consisted of scanning over a range of input current or diode temperature, and measuring the output power or frequency. This process was largely automated by computerized data collection from the wavemeter and temperature controller. The diode selected for the final implementation of this project was a AlGaInP quantum well laser diode (part number Sanyo DL4039-011).

The output power from the laser diode as a function of current has two linear regimes, as shown in Fig. 3-3. The slope increases sharply when the current reaches
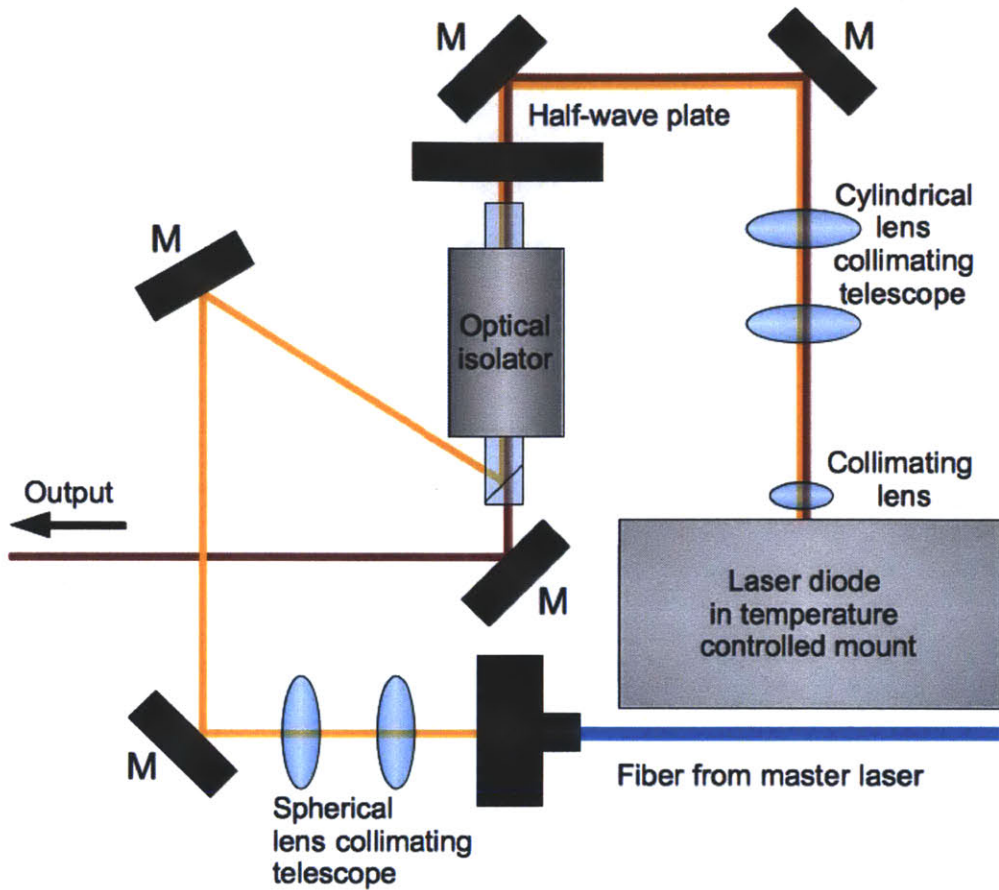
Figure 3-1: Diagram roughly to scale. The cylindrical lenses form a 2.5:1 telescope for the vertical axis with focal lengths of 50 mm and -20 mm, and the spherical lenses form a 2:1 telescope with focal lengths of 100 mm and -50 mm. M indicates a mirror.

a threshold value, $I_{thresh} \approx 40$ mA. The expected power of this laser diode, based on the datasheet, should be 10 mW. The measured power agrees with this value.

Although the frequency output of the laser diode is often linear with respect to small changes in temperature or current, sometimes the frequency will suddenly jump to a very different value, a phenomenon called mode hopping. This occurs because the frequency dependence is complicated and depends on many factors. Changing one factor at a time will cause mode hopping between maxima of the frequency response based on the other factors.

The output frequency of the laser diode decreases with increasing temperature.
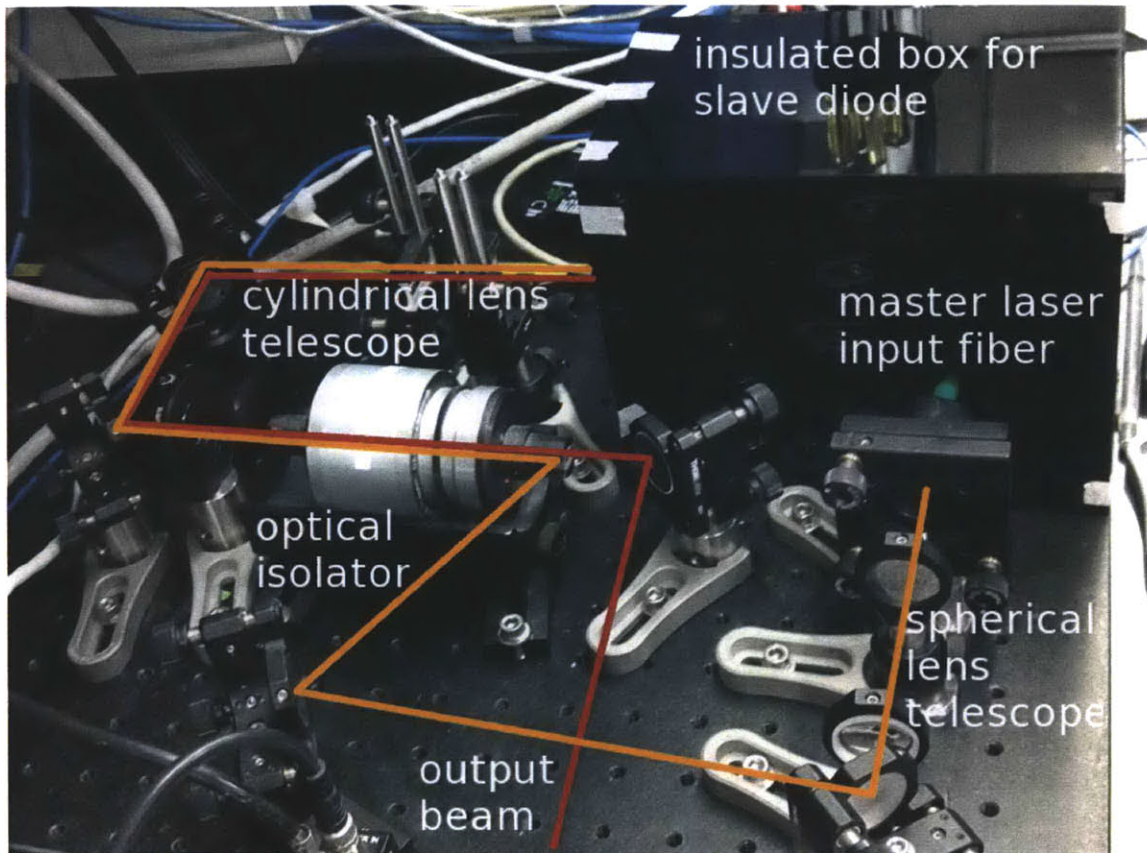
Figure 3-2: A photograph of the injection-locked laser setup, showing the insulated acrylic box housing the laser diode mount. The red line represents the output laser beam from the slave diode, and the orange line represents the injected laser beam from the master laser.

The decrease in frequency is smooth and linear while the diode remains within the same mode. When a mode hop occurs, the frequency will jump abruptly.

3.2.3 Optics equipment

Beam shaping and collimation

For injection-locking, the input and output beams must be well-overlapped and approximately matching in diameter. The output from the laser diode is highly divergent. A collimating spherical lens (f = 2.5 mm) placed directly in front of the diode forms an approximately elliptical, roughly collimated beam. A pair of cylindrical lenses (f = 50 mm and f = -20 mm) creates a telescope of magnification 2.5:1 to make
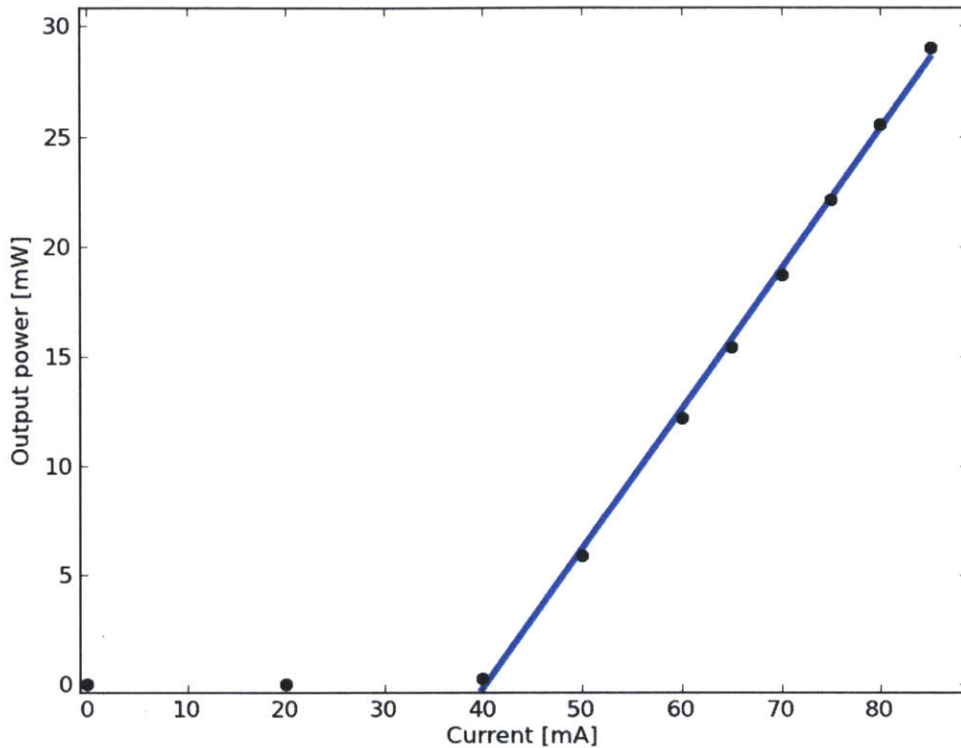
Figure 3-3: Measured output power as a function of current through the laser diode. The linear fit has a slope of 0.642 ± 0.003 mW/mA. The errors are based on the standard deviation of six measurements and the precision of the power meter, added in quadrature.

the beam into a round shape.

The input master laser beam was initially roughly collimated to a diameter twice as large as the output beam. This discrepancy in diameter was corrected by a telescope of two spherical lenses (f = 100 mm and f = -50 mm) with a magnification of 2:1.

To characterize the resulting shape of both beams, a spherical lens (f = 100 mm) can be placed in the roughly collimated beam to bring it to a focus. Since a Gaussian beam can be fully characterized by its beam waist at a focus and its divergence in the linear regime away from the focus, using the spherical lens means that the beam is much easier to characterize over a short distance with a beam profiler. Such a measurement of the master input beam is shown in Fig. 3-6 and of the free-running
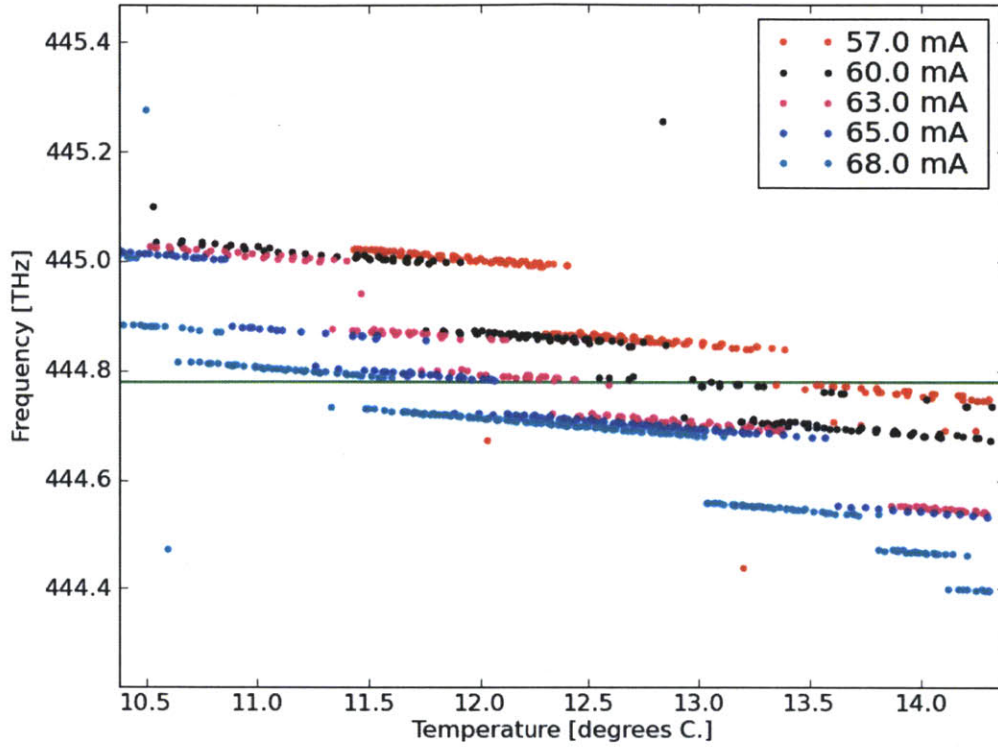
Figure 3-4: Variation in frequency output from a free-running laser diode over a range of temperatures and with different currents. Frequency generally decreases as the temperature increases, with a fixed current, or as the current increases, at a fixed temperature.

output beam is shown in Fig. 3-7.

Using the matrix model of the spherical lens, we can calculate the radius and divergence of the roughly collimated beams before they were focused. We solve

$$
\begin{bmatrix} r_f \\ r'_f \end{bmatrix} = M \begin{bmatrix} r_i \\ r'_i \end{bmatrix}
\tag{3.1}
$$

for r_i and r'_i, the initial beam radius and divergence before the beam passes through the spherical focusing lens. M is the matrix describing a spherical lens with focal
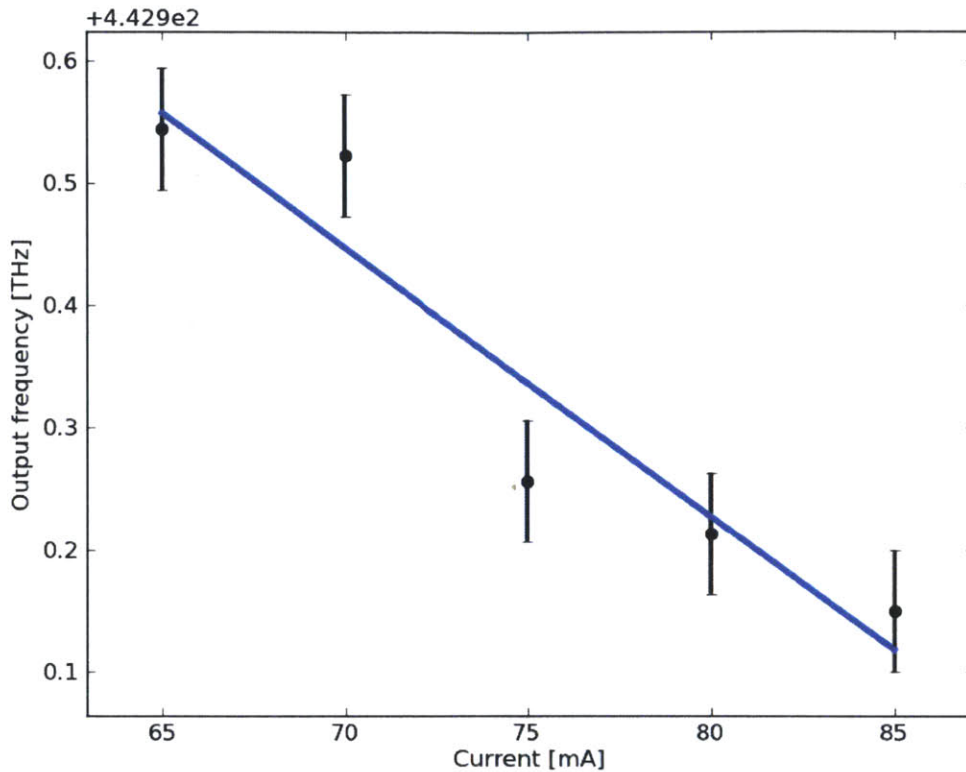
Figure 3-5: Measurements show that frequency of the laser diode decreases with increasing input current. Error bars are based on the standard deviation of three measurements. Slope of the linear fit = -22.0 ± 3.2 GHz/mA, with $\chi^2 = 1.8$.

length $f = 100$ mm:

$$M = \begin{bmatrix} 1 & 0 \\ -1/100 & 1 \end{bmatrix} \tag{3.2}$$

Based on the measurements of the focused beams shown in Fig. 3-6 and Fig. 3-7, the calculated values of the beam radii and divergence for the roughly collimated master and slave laser beams are listed in Table 3.1.

Optical isolator

The injection locked laser uses an optical isolator to prevent the output beam from back-propagating into the diode. The optical isolator is made out of a material that rotates the polarization of light when it is placed in a magnetic field, due to the
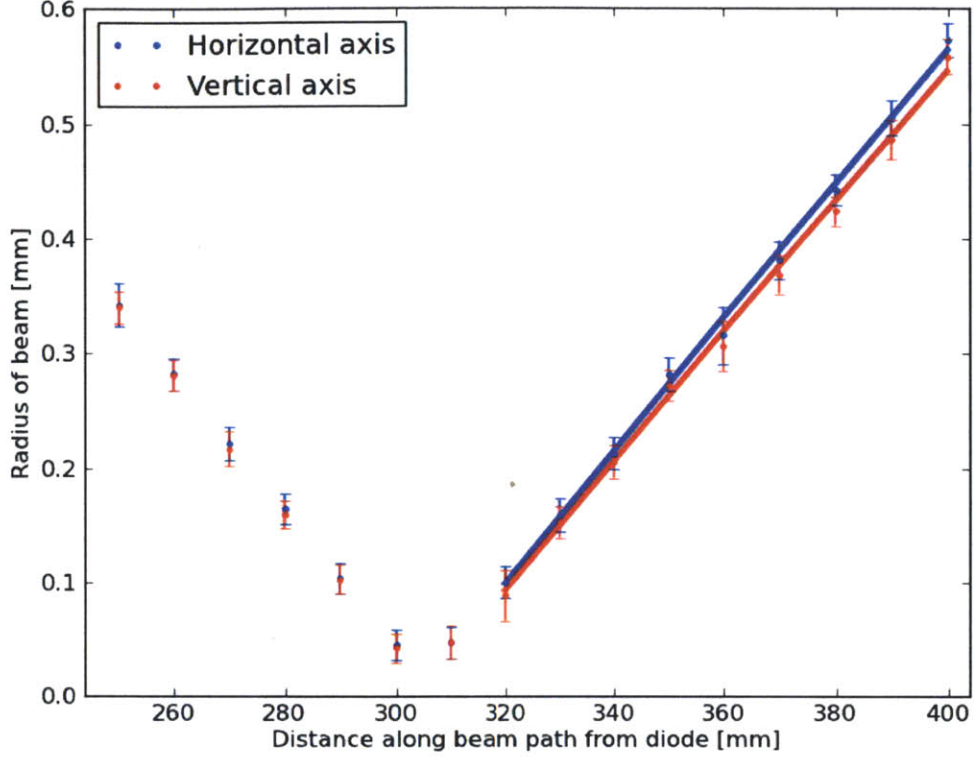
Figure 3-6: Beam profile of injected master laser beam, focused with $f = 100$ mm spherical lens. Half angle divergence (slope of linear fit) for horizontal and vertical profile, respectively: 0.0058 ± 0.0002, 0.0057 ± 0.0002. χ^2 for linear fit for horizontal and vertical profile, respectively: 0.2, 0.3. Beam waist at focus for horizontal and vertical profile, respectively: 0.045 ± 0.013 mm, 0.042 ± 0.013 mm.

	Radius [mm]	Divergence [no units]	M^2
Master beam, horizontal axis	0.625 ± 0.013	0.00045 ± 0.0002	1.2
Master beam, vertical axis	0.612 ± 0.013	0.00045 ± 0.0002	1.1
Slave beam, horizontal axis	0.527 ± 0.016	0.00057 ± 0.0002	1.2
Slave beam, vertical axis	0.417 ± 0.072	0.00057 ± 0.0009	0.96

Table 3.1: Parameters of the roughly collimated master and slave beams. Errors were propagated through the calculation from the errors on the divergence and beam radius measurements [BR03]. The value of M^2 for the vertical axis of the slave beam is likely unreliable due to the nonlinearity of the measured radius of this axis of the beam, even at a distance from the focus.

Faraday effect. The optical isolator currently used for the injection locked laser is made out of turbium glass, surrounded by a strong permanent magnet. The device
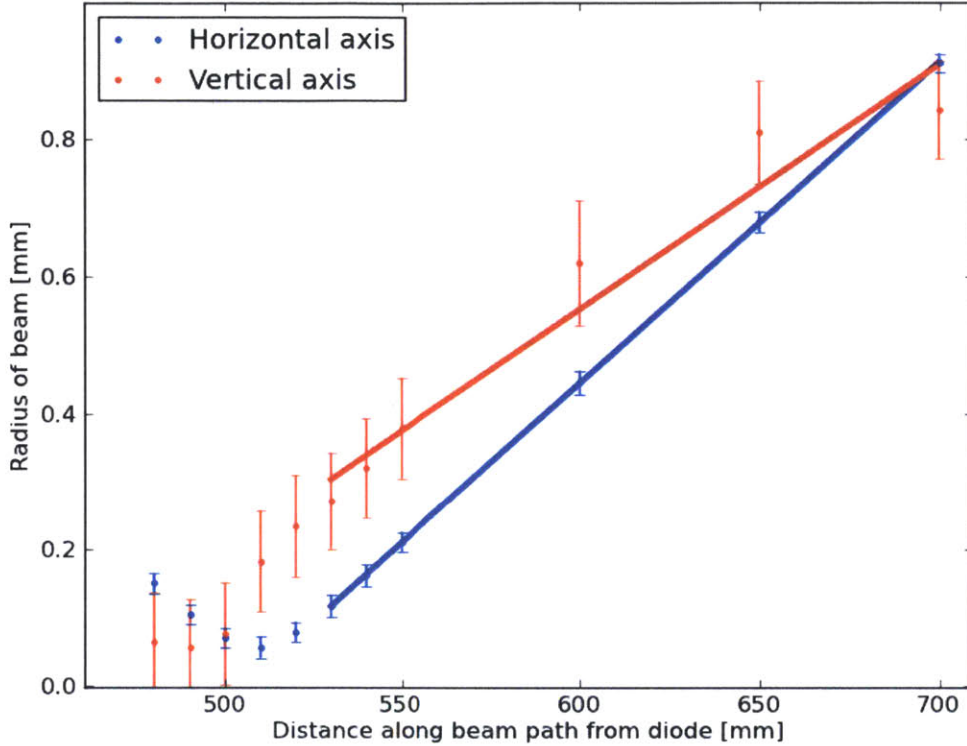
Figure 3-7: Beam profile of shaped output beam from slave diode, focused with $f = 100$ mm spherical lens. Half angle divergence (slope of linear fit) for horizontal and vertical profile, respectively: 0.0047 ± 0.0001, 0.0036 ± 0.0005. χ^2 for linear fit for horizontal and vertical profile, respectively: 0.01, 0.71. Beam waist at focus for horizontal and vertical profile, respectively: 0.057 ± 0.016 mm, 0.057 ± 0.072 mm.

is designed such that light passing through it changes polarization by 45 degrees.

The components of the optical isolator are shown schematically in Fig. 3-8. A polarizer is placed at the entrance of the optical isolator, causing the input light to be linearly polarized in one direction. To provide a concrete example, we can assume that the input light is linearly polarized at 0 degrees. Then, the polarization of the light passing through the optical isolator will be rotated until it is polarized at +45 degrees. Another polarizer with an angle of +45 degrees is placed at the exit. Any back-propagating light will reach the polarizer at the exit of the optical isolator and will be polarized to an angle of +45 degrees. The optical isolator will cause the polarization of this back-propagating light to rotate an additional 45 degrees, to +90

degrees. Since the polarization is now orthogonal to the polarizer at the upstream entrance, the back-propagating light will be absorbed.
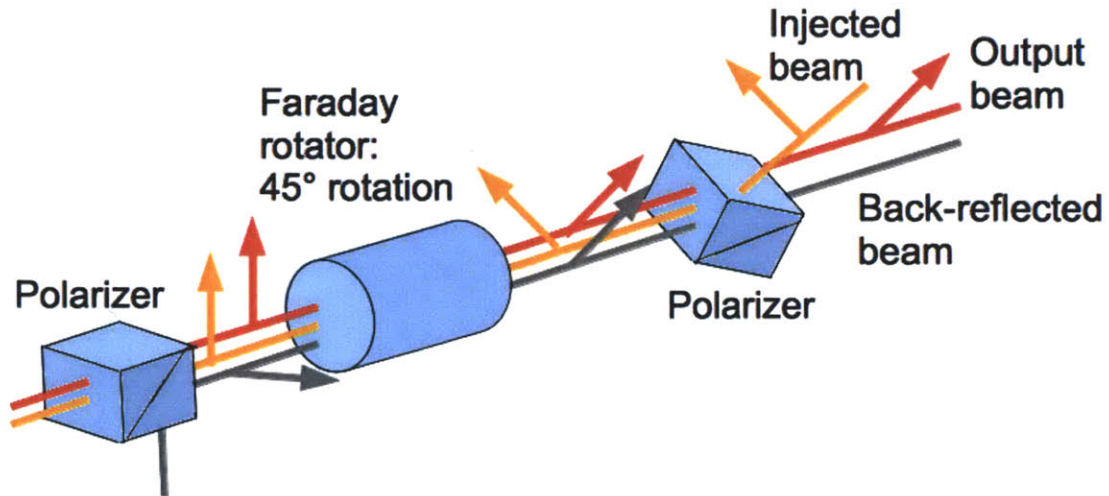
Figure 3-8: This diagram shows the main components of the optical isolator and their effect on the polarization and direction of an injected beam from the master laser, the output beam from the slave diode, and an unwanted back-reflected beam. The arrows indicate the direction of polarization of the electric field. The back-reflected beam may be randomly polarized initially, but the polarizer will allow only a component in one direction to pass through.

This kind of optical isolator is called polarization-sensitive. A polarization-insensitive optical isolator has a birefringent wedge at the entrance to separate the two orthogonal polarization components. The two separate components behave separately in essentially the same way as the light in the polarization-sensitive optical isolator. The advantage of the polarization-insensitive optical isolator is that it will work with any initial polarization of the light. Since in the injection-locked laser setup we have the freedom to choose the initial direction of polarization, a polarization-sensitive optical isolator is appropriate for this application.

Polarizing beam splitter cubes

Polarizing beam splitter (PBS) cubes are useful because they can output polarized laser beams that are not spatially offset. A PBS cube is composed of two right angle

prisms cemented together with a multilayer coating on one of the hypotenuse sides. Randomly polarized light directed at one side of the PBS cube will be divided into two polarized beams, with their polarization orthogonal to each other. If the PBS cube is oriented such that the long side of the cemented hypotenuse face is horizontal (the standard orientation in a beamline), the beam that is transmitted straight through will have horizontal polarization and the beam that is deflected at a 90 degree angle will have vertical polarization. The optical isolator uses a Glan-type PBS cube at both the entrance and exit of the device. The Glan-type PBS cube at the exit allows the injected master beam to approach the optical isolator at a sharp angle and pass through the device, coaligned with the slave beam.

Waveplate

A waveplate is a piece of birefringent material that can be used to change the polarization state of a beam of light. The phase velocity of light is faster along a given axis of the material and slower along the perpendicular axis (with both of these axes perpendicular to the beam of light.) As the light passes through the waveplate, the component of the beam polarized in one direction is delayed with respect to the other component. A quarter-wave plate and a half-wave plate have a difference in phase delay of $\pi/2$ and π, respectively.

Acousto-optic modulator

An acousto-optic modulator (AOM) is used to modify the output of a laser in a controllable way on a short time scale. Sending an acoustic wave through a material causes mechanical strain, which alters the index of refraction of the material [Hun09]. The resulting variation in the index of refraction is periodic. The periodic index of refraction in effect creates a grating which can cause an incident laser beam to change direction, frequency, or intensity. To test the injection-locked laser, an AOM was used to scan the master input laser over a frequency range to determine the locking range of the slave diode.

35

3.2.4 Temperature control

Temperature sensors

Three common types of temperature sensors are thermocouples, thermistors, and integrated circuit temperature transducers. Thermocouples are made out of wires made of two different conducting materials which produce a tiny voltage when pressed together at one end. This voltage is produced through the Seebeck effect and is linearly proportional to the temperature difference between the ends of the wires [VH86]:

$$\Delta V = \alpha_S \Delta T \tag{3.3}$$

where ΔV is the voltage produced, ΔT is the temperature difference between the ends of the wires, and α_S is the Seebeck constant.

A thermistor is a device with temperature-dependent resistance. The resistance varies linearly with temperature, with a negative slope:

$$R = R_0 - R_1 T \tag{3.4}$$

where the resistance R is a function of two constants, R_0 and R_1, and the temperature T.

The IC temperature transducer is similar to a transistor. It acts as a temperature-dependent current source. The current output can be described by:

$$I = I_0 + I_1 T \tag{3.5}$$

where the current I is a function of two constants, I_0 and I_1, and the temperature T. The IC temperature transducer can also be modeled as a thermistor:

$$I = \frac{V}{R_0 - R_1 T}. \tag{3.6}$$

It requires a bias voltage applied in series and a meter to measure the current. A bias voltage applied in parallel will not work, as the device will not change the current in

the circuit in this case. We used an IC temperature transducer (part number AD590) in this application since it offers more precision than a thermocouple.

Thermoelectric cooler

Thermoelectric devices convert electrical energy into a temperature gradient using the Peltier effect [RM03]. A thermoelectric cooler (TEC) is composed of one or more pairs of n- and p-type semiconductors. Heat is absorbed when electrons travel from a lower energy level in the n-type semiconductor to a higher energy level in the p-type semiconductor. Such a device has no moving parts and serves as a very reliable and controllable heating or cooling element for controlling the temperature of a laser diode. A TEC is incorporated into the laser diode mount selected for this project.

Automated temperature control

A Wavelength Electronics temperature controller, model number PTC-2.5K, regulates the current passing through the TEC element by using a proportional-integral-derivative (PID) control loop. The desired temperature may be adjusted by varying an analog input voltage:

$$T = \frac{V - 2.730}{0.01} \tag{3.7}$$

where T is the desired temperature in degrees Celsius and V is the voltage in volts. The required voltage stability of the input analog source can be calculated. The laser diode should be stable to within $\Delta f = 1$ GHz. The temperature controller changes the temperature by $\gamma = 100$ K / 1 V. Over a wide range, the frequency changes with temperature by $\alpha \sim 150$ GHz / 1 K. Within a single mode, the frequency changes with temperature by $\beta \sim 30$ GHz/K. The voltage stability based on α is:

$$\Delta V_\alpha = \frac{\Delta f}{\alpha \gamma} = \frac{1 \text{ GHz}}{150 \text{ GHz/K} \times 100 \text{ K/V}} = 0.07 \text{ mV} \tag{3.8}$$

and the voltage stability based on β is:

$$\Delta V_\beta = \frac{\Delta f}{\beta \gamma} = \frac{1 \text{ GHz}}{30 \text{ GHz/K} \times 100 \text{ K/V}} = 0.3 \text{ mV}. \tag{3.9}$$

The reference input voltage to the temperature controller must be stable within these limits to adequately prevent temperature fluctuations.

Dew point concerns and humidity control

The frequency emitted by the laser diode is strongly temperature dependent. The laser diode used for this project reaches the correct frequency at approximately 13 degrees Celsius. Since this is well below room temperature, we had initial concerns that the diode might be running below the dew point, which means condensation could form on the diode from the water vapor in the air. Condensation could destroy the diode.

If the diode temperature is below the dew point, a function of the ambient air temperature and relative humidity, water vapor will condense out of the air. At a relative humidity of 100%, the dew point is equal to the ambient temperature by definition. The dew point can be estimated by various methods, for example as described by Lawrence [Law05]. Fig. 3-9 shows how the dew point varies with relative humidity at an ambient room temperature of 24 degrees Celsius.

Since the relative humidity in lab is typically 15-19%, and was observed to reach no higher than 23% last August, during normal lab conditions the temperature of the laser diode will be above the dew point. Even so, we decided to include silica desiccant as a safeguard inside the insulating box surrounding the laser diode mount, to absorb anomalous water vapor.

3.3 Demonstration of injection-locking

After the parts of the apparatus were mounted on an optics breadboard and aligned, the input and output beams were measured with a beam profiler. Lenses were installed to shape the beams to approximately the same dimensions. We adjusted the temperature and current such that the frequency output from the free-running laser diode was close to the desired frequency. When the beam from the master laser was introduced, injection-locking behavior was apparent. The output frequency jumps to
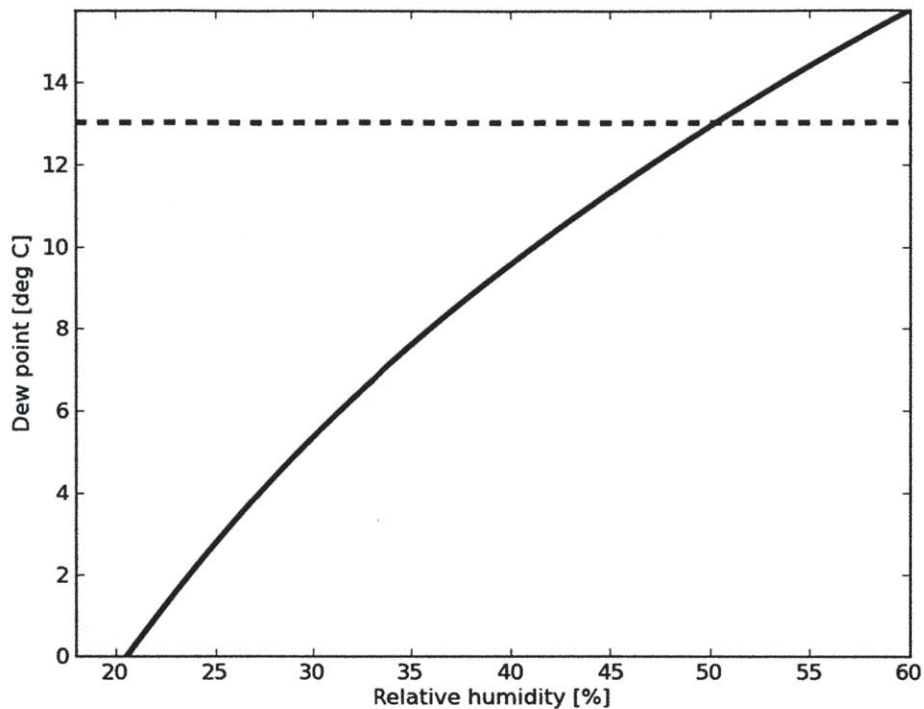
Figure 3-9: The solid curve represents the dew point at an ambient temperature of 24 degrees Celsius, and the dashed line is at 13 degrees Celsius, the desired temperature at which to run the laser diode. The desired temperature is comfortably above the dew point if the relative humidity remains below 45%.

a value near the input frequency and remains there while the frequency is within the locking range.

The approximate settings for the free-running diode to be in the correct mode are a temperature of 13.3 ± 0.2 degrees C. and a current of 58.5 ± 0.5 mA. The temperature and current settings must be empirically adjusted until the diode settles into the correct mode. When the diode injection locks, the increased power generated heats up the diode. This sometimes causes the diode to fall out of lock. Time or further adjustments will then be necessary to return the laser to a locked state.

Once the laser is locked to the injected frequency, the injected beam was scanned over a range in frequency in order to test the injection-locking range. An acousto-optic

modulator was used to adjust the injected master frequency. Data from scanning the master frequency across the locking range is shown in Fig. 3-10. Data from the same scan plotted only within the locking range is shown with a smaller vertical scale in Fig 3-11 to demonstrate the stability within the locking range. The measured locking range of 18.4 ± 1.6 MHz is much smaller than the locking range of 800 MHz found by Clarke, Riis, et al. for a laser diode at the same output frequency [CRB98]. It is likely that the locking range for the diode could be increased with increased injected power, combined with more stable temperature control. The locking range can be shifted up or down in frequency by a small adjustment in the laser diode current.

The input laser power from the master laser required for injection-locking is 9 ± 2 μW. A much larger injected power causes too much heating of the diode, causing the slave laser to oscillate in and out of lock. The output power of the diode before the beam passes through the optical isolator is 11.56 ± 0.31 mW. The ratio of the injected power to the output power is $(7.8 \pm 1.7) \times 10^{-4}$, with the errors propagated appropriately through the calculation [BR03].
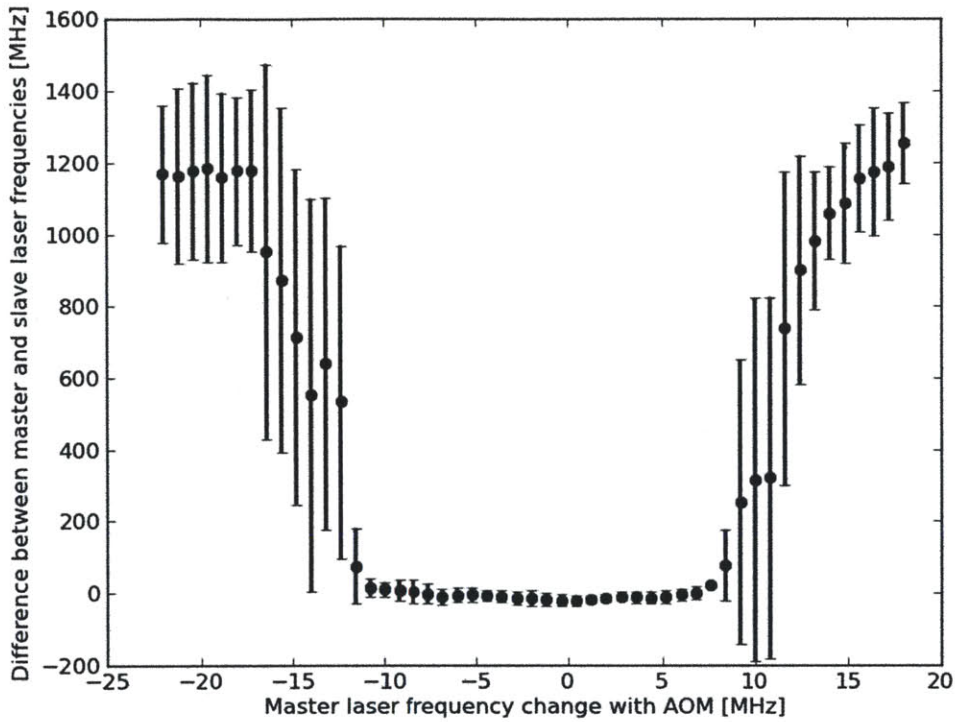
Figure 3-10: An injection-locking range of 18.4 ± 1.6 MHz is demonstrated by scanning the input master frequency and observing how closely the slave frequency follows. The graph shows the results of scanning the master laser from a frequency below the locking range to a frequency above the locking range and back, twice. The master laser is centered on 444.779044 THz. Before the scan, the laser diode current was adjusted empirically until the output stabilized in the correct mode, injection-locked to the master laser. It is evident that for a range in master frequency, the slave frequency abruptly jumps very close to the master frequency. Fig. 3-11 plots the data within the injection-locking range in more detail.
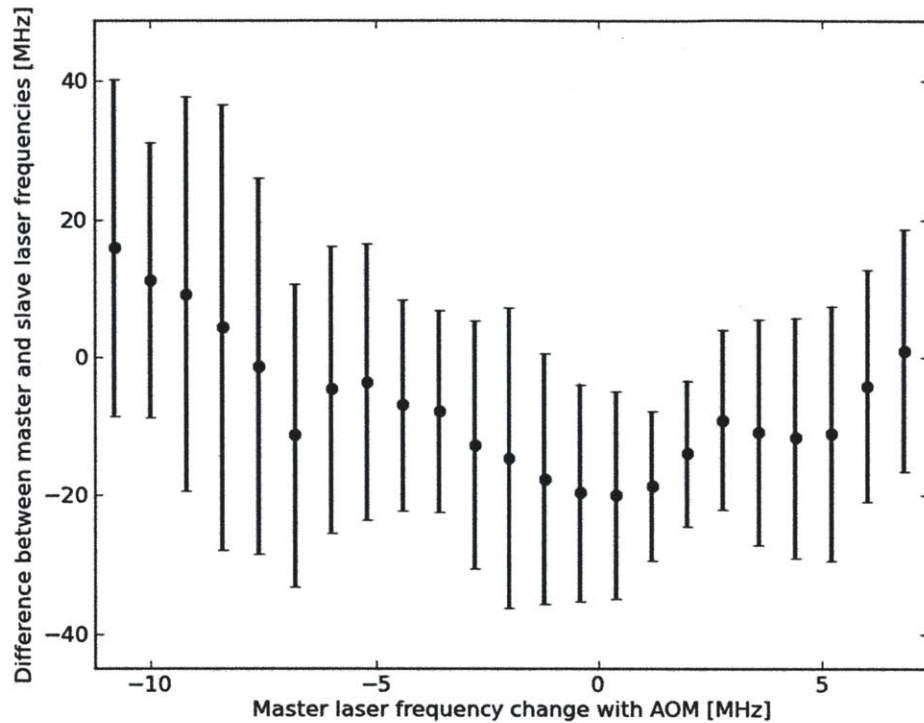
Figure 3-11: The same data over the injection-locking range that are shown in Fig. 3-10. This graph only shows points within the injection-locking range to demonstrate frequency stability within the range. The slave laser frequency was observed to drift higher in later scans. After some time, the slave laser failed to lock in this range until the current was adjusted. The resolution of the High Finesse WS-7 wavemeter used for these frequency measurements is about 40 MHz, so the errors (based on the standard deviation of four measurements) are likely a demonstration of this limitation of the precision.

Chapter 4

Conclusions

A major goal of experimental quantum information processing is to create reliable, scalable systems for storing, manipulating, and reading out data using a quantum system. Powerful, stable lasers are an essential part of realizing this goal for ion trapping systems. The injection-locked laser described in this thesis provides a power amplification of a factor of 1200, with an ouput power of 11.56 ± 0.31 mW. The increased power will speed up Rabi oscillations of the qubit transition between energy levels in the $^{88}Sr^+$ ion. The observed injection-locking frequency range of the laser diode is 18.4 ± 1.6 MHz. This range can be shifted up or down in frequency by adjusting the laser diode current.

4.1   Future improvements

The free-running frequency of the laser diode is highly dependent on its temperature. If the laser diode is not sufficiently insulated from the outside environment, air currents and ambient changes in temperature in the lab will cause the laser to fall out of lock. The stability of the laser was greatly improved with an insulated acrylic box surrounding the diode mount. An additional outer box surrounding the entire setup would contribute to additional temperature stability. The outer box could be lined with foam and include rubber along the bottom and top seams in an effort to make it more airtight.

The present voltage supply used as a reference for the temperature controller is an Agilent E3630A DC power supply. If it turns out that the voltage stability is the limiting factor for ensuring temperature stability, a more stable power supply could be installed.

A novel method of controlling the temperature of a laser diode using the included packaged photodiode was demonstrated by Andreoni and Xu [AX00]. Running a DC current through the photodiode produces a predictable power dissipation which can be used to heat the laser diode. Due to the low thermal capacity of the laser diode package, the photodiode can rapidly change the temperature of the laser diode, much more quickly than the standard TEC element in the diode mount. The fast temperature change resulting from the photodiode heating could be combined with the more powerful TEC element to achieve increased temperature stability.

For ion trapping, it will be important to characterize the quality of the output beam from the injection-locked laser in terms of frequency stability, linewidth, and noise. The increased power from the injection-locked laser acting on the $^{88}Sr^+$ ion qubit transition will be useful for quantum computations requiring a number of operations within the coherence time of the ion, or operations entangling two or more ions.

Bibliography

[AX00]   E. Andreoni and J. H. Xu. A simple system of thermal control and fre-
           quency stabilization of solitary diode lasers. *Review of Scientific Instru-
           ments*, **71**(10), 3648–3652, 2000.

[BMD04]   B. B. Blinov, D. L. Moehring, and L. M. Duan. Observation of entan-
           glement between a single trapped atom and a single photon. *Nature*,
           428(March), 153–157, 2004.

[BR89]   D. P. Bour and A. Rosen. Optimum cavity length for high conversion
           efficiency quantum well diode lasers. *J. Appl. Phys.*, **66**(7), 2813–2818,
           1989.

[BR03]   P. R. Bevington and D. K. Robinson. *Data Reduction and Error Analysis
           for the Physical Sciences*. McGraw-Hill, 2003.

[CRB98]   R. B. M. Clarke, E. Riis, and G. P. Barwood. A sideband-injection locked
           extended cavity diode laser for interrogating cold trapped Strontium ions.
           Optics Communications, **158**(1-6), 36–40, December 1998.

[CVZ+98]   I. L. Chuang, L. M. K. Vandersypen, X. Zhou, D. W. Leung, and S. Lloyd.
           Experimental realization of a quantum algorithm. *Nature*, **393**(6681),
           143–146, May 1998.

[Gol86]   P. Goldsmith. Gaussian beam transformation with cylindrical lenses. *An-
           tennas and Propagation, IEEE Transactions*, **2**(4), 603–607, 1986.

[GRL+03] S. Gulde, M. Riebe, G. P. T. Lancaster, C. Becher, J. Eschner, H. Häffner, F. Schmidt-Kaler, I. L. Chuang, and R. Blatt. Implementation of the Deutsch-Jozsa algorithm on an ion-trap quantum computer. *Nature*, **421**(6918), 48–50, January 2003.

[Hun09] R. G. Hunsperger. Acousto-Optic Modulators. In *Integrating Optics*, pp. 201–220. Springer US, New York, NY, 2009.

[KMW02] D. Kielpinski, C. Monroe, and D. J. Wineland. Architecture for a large-scale ion-trap quantum computer. *Nature*, **417**(6890), 709–711, June 2002.

[Law05] M. G. Lawrence. The Relationship between Relative Humidity and the Dewpoint Temperature in Moist Air: A Simple Conversion and Applications. *Bulletin of the American Meteorological Society*, **86**(2), 225–233, February 2005.

[LGA+08] J. Labaziewicz, Y. Ge, P. Antohi, D. Leibrandt, K. Brown, and I. L. Chuang. Suppression of Heating Rates in Cryogenic Surface-Electrode Ion Traps. *Physical Review Letters*, **100**(1), 1–4, January 2008.

[MMKI95] C. Monroe, D. M. Meekhof, B. E. King, and W. M. Itano. Demonstration of a Fundamental Quantum Logic Gate. *Physical Review Letters*, **75**(25), 4714–4717, 1995.

[NLR+99] H. C. Nägerl, D. Leibfried, H. Rohde, G. Thalhammer, J. Eschner, F. Schmidt-Kaler, and R. Blatt. Laser addressing of individual ions in a linear ion trap. *Physical Review A*, **60**(1), 145–148, 1999.

[Pau90] W. Paul. Electromagnetic traps for charged and neutral particles. *Rev. Mod. Phys.*, **62**(3), 532–540, 1990.

[RM03] S. B. Riffat and X. Ma. Thermoelectrics: a review of present and potential applications. *Applied Thermal Engineering*, **23**(8), 913–935, June 2003.

[Sie86] A. Siegman. *Lasers*. University Science Books, 1986.

46

[SS66]   H. L. Stover and W. H. Steier. Locking of Laser Oscillators By Light Injection. *Applied Physics Letters*, **8**(4), 91–93, 1966.

[TRBZ04] L. Tian, P. Rabl, R. Blatt, and P. Zoller. Interfacing Quantum-Optical and Solid-State Qubits. *Physical Review Letters*, **92**(24), 2–5, June 2004.

[VH86]   A.W. Van Herwaarden. Thermal sensors based on the Seebeck effect. *Sensors and Actuators*, **10**, 321–346, 1986.

[VSB01]   L. M. K. Vandersypen, M. Steffen, and G. Breyta. Experimental realization of Shor's quantum factoring algorithm using nuclear magnetic resonance. *Nature*, **414**, 883–887, 2001.